

Application Methods for Self Organizing Map in Process Imaging for Dynamic Behavior of Aerated Agitation Vessel

Hideyuki Matsumoto, Ryuichi Masumoto and Chiaki Kuroda
Department of Chemical Engineering, Tokyo Institute of Technology
E-mail: hmatsumo@chemeng.titech.ac.jp

Abstract

The batch Self Organizing Map, abbreviated to SOM, is adapted to process imaging for dynamic behavior of aerated agitation vessel, and the application methods are investigated in this article. In the application, the direct imaging by CCD video camera and the PIV technology are adopted. As a result of mapping time-series patterns of velocity distributions to two dimensions, it is shown that generated map and clusters could give process engineers useful information about degree of spatial dispersion of bubbles and about determination of design parameter. The next, two approaches for the data processing in the SOM are investigated to enhance efficiency of pattern analysis: phenomenological approach and statistical approach. As to the statistical approach, it is found that adoption of sigmoid transformation enhances the efficiency of separating the minor difference in the nodes representing the “well-dispersion” patterns and that it would give process engineers useful information about transition of process patterns.

1. Introduction

In chemical process industry, local sensors cannot always give us sufficient information for estimating the overall dynamic behaviors inside a chemical reactor. Therefore process engineers often apply soft sensors as typified by neural networks [1] for process monitoring and control. Soft sensors based on the black box model are considered to be practical methods. On the other hand, software of computational fluid dynamics (CFD) gives us much information about distribution of process inside the reactor on the basis of solving first-principle model [2].

Recent speedup of processor and advance of graphic user interface (GUI) technology facilitate the

engineers using commercial CFD software. It is, however, difficult to implement an accurate simulation for complicated flow regimes such as multiphase flow and reactive flow. There is a problem that computational time increases with meshes, especially when geometrical structure inside reactor is complicated. As a method for solving the problem, we proposed application of hybrid simulation where CFD simulation and process simulation was combined [3]. It was considered that the proposed method was practical for process design, but not practical for process control for reason of long simulation time.

Thus it is supposed that data-driven model based on 2D or 3D image inside a reactor is applicable to monitoring and control of the distributed parameter system.

Process imaging is well known as an effective methodology for pattern recognition and automatic control of the distributed parameter system. Figure 1 shows a framework of procedure in process imaging, which consists of five steps, which are described by D.

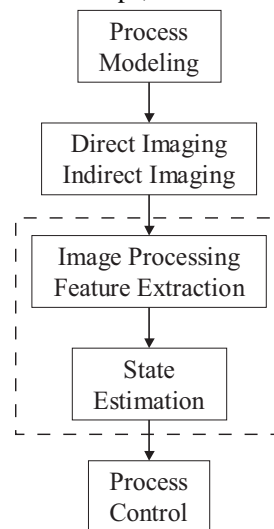


Figure 1. Steps involved in process imaging for a control application

M. Scott et al. [4]. If process dynamics can be analyzed by physicochemical model, the process modeling could enhance efficiency of processing in the next steps. In the data acquisition, there are two methods: “direct imaging” and “indirect imaging.”

Recently, Process Tomography (PT) is known as a good method of imaging flow pattern inside equipment indirectly [4]. A typical PT technique is based on measurements of electrical properties that are capacitance, resistance and impedance. Many applications of the PT have been studied in laboratory scale and pilot plant scale. For example, the electrical tomographies could provide detailed information about spatial distribution of gas-liquid mixing in a stirred vessel [5], and about distribution of the void fraction that is related to gas holdup in a bubble column [6]. It was reported that phase distribution obtained by the tomographic imaging could be useful information for control of polymerization process [7]. In mass-produced applications, the PT in the present time has some problems, which are related to complexity and specificity of sensor elements and to their need for close integration into process.

On the other hand, direct imaging system is thought to be a simple, because it does not rely on mathematical reconstruction to form an image. Advance of CMOS sensor and CCD technology in a few decades realizes direct imaging that is inexpensive and quality. One of applications of the direct imaging technique to chemical process is flotation froth monitoring [8, 9]. It is widely known that color and morphology of the froth are closely related to mineral concentrations and process status. So process imaging has been considered as a potentially key component to the process monitoring. In the process imaging for monitoring and control, image processing and feature extraction are important. That is to compile an enormous amount of data in the distributed parameter system. It has been reported that Principal Component Analysis (PCA) is a useful statistical method in the feature extraction [9]. In addition to the statistical methods, it is well known that an intelligent system technology is effective in extracting complex interaction between process data and operation variables, which shows a nonlinear nature.

In this article, Self Organizing Map, abbreviated by SOM, is considered to be useful intelligent system for the process imaging. SOM proposed by Kohonen is one of neural networks where unsupervised learning algorithm is adopted [10]. By using SOM, feature of input data can be extracted automatically and a map for clustering the feature is self organized. SOM has ability to project high-order dimensional data to the two dimensions that is a plane, so that visualization of

high-order dimensional space is possible. Kohonen has reported that the number of academic papers for the SOM, which are related to analysis of the algorithm, its extension and application, is over 4000 in his book [10]. In the industrial fields, this method of data processing can be utilized in much recognition of image, speech and fingerprint. As to process monitoring and control, applications of the SOM have been investigated for different chemical processes: copper flash smelting process [11], suspension ethylene polymerization process [12], wastewater treatment process [13], froth flotation process [14]. For monitoring of fermentation process, combination of the SOM and process image was reported [15]. Process image of spectrogram was obtained by the two-dimensional (2D) fluorescence sensor, as one type of optical sensor. It was also reported that the SOM-based classification of the spectral data was effective in modeling the process by a supervised neural network [16]. Therefore it is considered that the SOM is powerful tool for pattern recognition in process imaging, which is related to the steps inside the box drawn by dash line in Figure 1.

In this article, we apply the SOM to clustering multiphase flow in stirred-tank reactor, which is a difficult case for the CFD simulation. An aerated agitation process is specified as the process of multiphase flow. The aerated agitation is applied to enhancing efficiency of gas absorption to liquid by dispersing gas bubbles in the vessel, which is, for example, exploited in bio industrial equipment known as a “jar fermentor”. Pattern recognition and estimation of dispersion of bubbles is significant for monitoring of dynamic behavior of gas absorption, although the dispersion is generally evaluated as the average amount of “gas hold-up” by measuring change of liquid level. The pattern of gas dispersion in the agitation vessel is changed with time nonlinearly and periodically, and it is considered that analysis of the pattern transition may give process engineers useful information about dynamic behavior of the overall process.

Hence, a purpose of this study is to propose a clustering method based on the SOM for monitoring dynamic behavior of distribution of bubbles. In the data acquisition, the direct imaging by CCD camera is adopted with a method of PIV (Particle Imaging Velocimetry), which will be explained in detail in the next section. Then another purpose is to investigate methods of enhancing efficiency of the pattern analysis from the viewpoints of data processing and parameter setting of the SOM. Two approaches that are phenomenological approach and statistical one are applied to modification of the proposed clustering

method in this article. Through these investigations, we will discuss applicability of the SOM to process imaging for monitoring and controlling dynamic behavior inside a chemical reactor.

2. Direct imaging of bubbles' flow inside an aerated vessel

2.1 Data acquisition system by direct imaging

Figure 2 shows a setup of experimental system for the aerated agitation process. Inside the cylindrical vessel of which interior diameter is 190 mm, four baffles are placed for mixing fluid well. The vessel is made in acrylic resin to do experiment under conditions of high visibility. Test fluid inside the vessel is water, and nitrogen that is insoluble to water is used as an aeration gas. The aeration is carried out by the ring sparger installed at the bottom of the vessel. The sparger has sixteen air holes on surface of the ring, and nitrogen gas is supplied at constant flow rate 0.6 L/min by mass flow controller. And paddle-type impeller with six blades, of which diameter is 60 mm, is set up at height of d from the bottom. The value of d is changed for the later pattern recognition.

In this article, light sheet is used for enhancing edges of bubbles, so that it could increase accuracy of data processing in the following PIV. The light sheet is generated by a DPSS (Diode-Pumped Solid-State) laser, "excel" (Laser Quantum Ltd.) that produces a

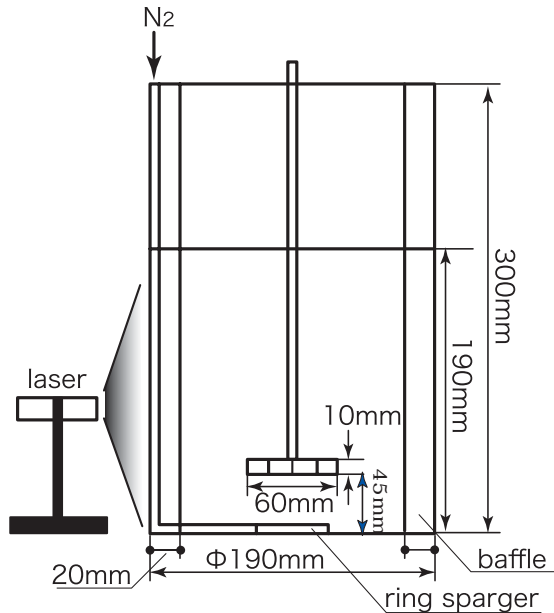


Figure 2. Schematic diagram of an experimental system

high power green beam whose wavelength is 532 nm. In order to form a clear plane of the light sheet, the position of the plane is determined so as to avoid light scattering due to the impeller shaft and the baffles. And, the motions of bubbles entrained in the flow are recorded by a digital video camera recorder, which is oriented at 90 degree to the plane of the light sheet. The digital video camera recorder used first in this article is DCR-VX2000 (Sony Corp.), which has mega-pixel CCD and CMOS sensor. Frame rate in the recording is set at 30 fps.

As an experimental result for this study, Figure 3 (a) and (b) show continuous frames of gas dispersion through binarization, in which white areas indicate existences of bubbles. Parts of the impeller, its shaft and the sparger are masked. The two frames, of which the time difference is 1/30 sec corresponding to frame rate of the video camera, are computed by PIV described in the next subsection.

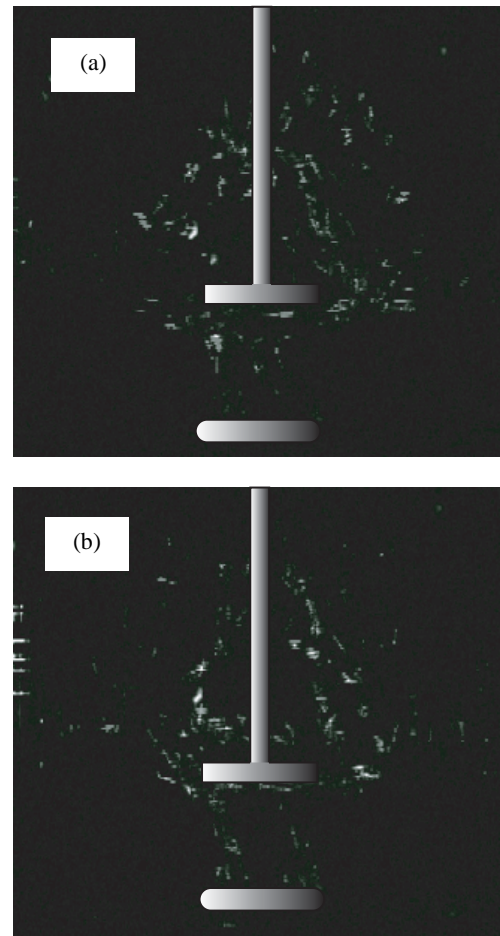


Figure 3. An example of continuous frames of gas dispersion

2.2. Application of Particle Imaging Velocity (PIV)

In image recognition of object's motion, there are mainly two methods. One method is based on difference between two freeze-frame pictures. Another one is based on velocity vector of object, which is estimated from moving images. PIV technology is known as the latter method and is popular for flow pattern visualizations for many cases: air flow around vehicle, flow inside tank and so on. Typically minute particles are added to flow for the visualization, as assuming that each particle moves at local velocity of the flow. Distribution of particles on a cross section that are visible by the above-mentioned light sheet is shot by CCD video camera.

Each of two exposures by the video camera is recorded on a separate frame. Frame converted into numbers such as values of RGB is devised into small space domains, what is called "test areas". By computing cross-correlation of the two frames with respect to the test areas, a vector of local displacement of the particle image can be estimated. The vectors of local displacement of image can be converted into two component vectors of local velocities in a flow, as considering time difference of the two frames and a scaling factor of the frame.

In this article, we used commercial software of "PIVview 2C ver. 2.3" (PIVTEC GmbH). In the application of PIV, it was considered that wide computational domain influences increase of computational time and detection of noise e.g. reflections of the light on wall of the vessel and on the water surface. Actually, the detection of much noise was seen in a case when the computational domain is the overall vessel. Thus we determined the domain as depicted by the box in Figure 4, in assuming that bubbles would be dispersed almost symmetrically in the vicinity of the impeller's shaft. Frames of the computational domain were divided into multiple cells to estimate vector of local displacement of the bubble image. Size of each cell, in this study, was set at 5.7mm x 5.7mm, by taking consideration into averaged size of bubbles that was estimated in the prior experiments. Hence the number of cells was 207, which was composed of 9 cells wide and 23 cells row.

Figure 5 illustrates an example of results of PIV processing. Tone inside the box in the right part of the figure indicates distribution of magnitudes of velocities. Since transition of such the process image is analyzed by the SOM in this article, multiple process images are recorded at a time interval of 0.2 sec, as depicted by Figure 6. As we see distributions of tone changing

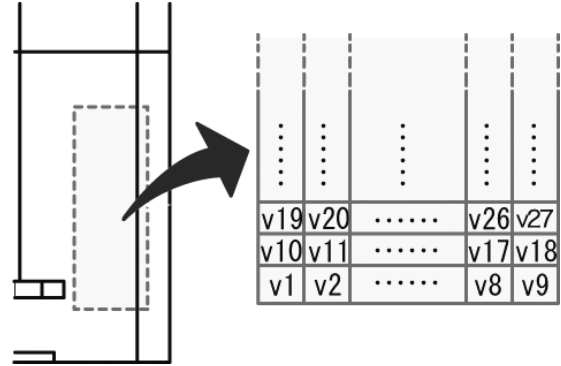


Figure 4. Schematic diagram of computational domain and cells divided for application of the PIV



Figure 5. An example of velocity distribution estimated from continuous frames

with elapsed time, it seems that the direct imaging method described in this section was applicable to acquisition of patterns for flow of bubbles.

3. Batch Self Organizing Map

In this article, we used "Viscovery[®] SOMine ver. 4.0" (Eudaptics Software GmbH), which was based on the concept and algorithm of the batch SOM introduced by T. Kohonen [10]. In the SOMine, two-dimensional Kohonen nets are used.

In the original SOM algorithm, each node has a weight vector w . The components of this vector represent the strength of the synapse connections to the input neurons. The Kohonen algorithm enables these weights to adapt themselves in response to the input signals as follows.

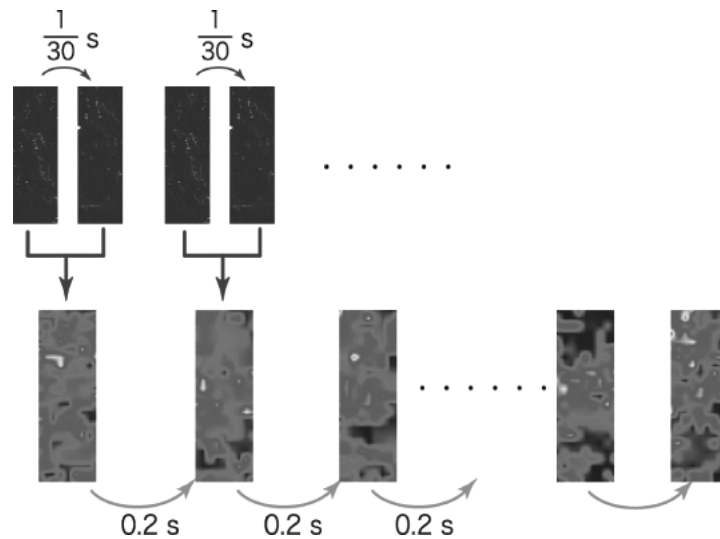


Figure 6 . A set of process images for the SOM

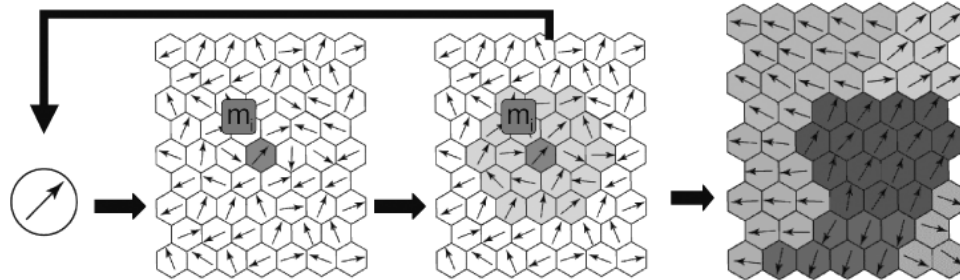


Figure 7. Schematic diagram of training process in the original SOM

- The winner node c changes its weight vector w_c to become more similar to the input vector x
- All neighbors of c which lie within a predefined distance to the winner node also change their weight vector to the direction of x

This modification is proportional to the difference between the input vector x , and the corresponding weight vector.

Figure 7 shows a schematic diagram of “sequential” training in the original SOM. The first, searching of a node that is matched best to a data vector is carried out, which is called “Matching”. Matching is performed by computing the distance between the data vector and each node vector in the map. The data vector is assigned to the node m with the smallest Euclidean distance. As the next step, the training algorithm sets the node m , which is shown in Figure 7, to the weighted mean of all data vectors that matched to the nodes in the neighborhood of node m . The weight for a data vector is determined based on the distance (in map space) between the node m and the neighboring node where the data vector matched. Thus, the two steps are

iterated, so that the distortion and the quantization error are minimized.

In contrast to the original SOM algorithm, the batch SOM algorithm first processes all data vectors, and then updates the map once. It is said that the batch SOM algorithm is faster and more robust than the original Kohonen algorithm. In the Viscovery® SOMine [17] based on the batch algorithm, the initial data vectors are set up by the principal component analysis (PCA) of the input data that are training data. That is to say, training in this article starts from a map representing linearized space for the multi-dimensional input data. Topological connection between arbitrary two nodes is defined by the Gaussian function. The radius of the Gaussian function is called “Tension” in the SOMine, which is used for determining degree of smoothing the map. Then, in training of the map, the SOMine updates a node vector by setting it to the mean value of all weighted data vectors that matched to that node and its neighboring nodes, in a way of the K-means method. During the training process, the number of node in a map is not fixed but grows from a fairly small number to the desired number of nodes, in

order to implement more efficient training. Each map is trained for a certain number of batches using a decreasing tension. When the number of nodes is increased, the growth of the map is compensated by a corresponding increase of the tension.

4. Results and discussions

4.1. Clustering of dynamic behaviors of bubbles

207 velocity vectors are acquired from the two frames by using the PIV, as shown in Figure 4. Each velocity vector is two dimensional because of making an exposure by the light sheet. In this article, magnitude of the vector was used as an input. So the data vector for the SOM consisted of 207 magnitudes of the velocities. We prepared 30 data vectors, which represent images recorded at a time interval of 0.2 sec., in an operational condition.

In the training process, values of each component was scaled to the range $-1/\sqrt{n}$ and $1/\sqrt{n}$. The desired number of nodes was set at 2000, and the final value of tension was 0.5. In clustering after the training, the SOM-Ward clusters were used. This clustering method combines the local ordering information of the map with the classical hierarchical cluster algorithm for Ward. Viscovery[®] SOMine computes an indicator for each element of this hierarchical sequence of clustering, which indicates a quality measure for each count. If the indicator is high for a particular cluster count, it can be interpreted that the clustering may be viewed as “natural” for the map.

The first, for the case that rotational speed of the impeller N was 200 rpm and its height d was 30 mm,

different 30 images were classified by the above-mentioned batch SOM. As a result of the mapping, a map separated into four clusters is depicted in Figure 8. Both of the distortion and the quantization error were almost zero, which showed good mapping. When the cluster count was four, the indicator was 15, which was high as compared with the other cluster count. Four schematic drawings around the map in Figure 8 show specific patterns of gas dispersion for the clusters. As observing the frame for a data vector matched to a node best, it could be interpreted that the cluster in the left lower part of the map showed process image where many bubbles were dispersed inside overall the vessel. On the other hand, the cluster in the right part was interpreted to show a group of images where few bubbles were dispersed.

Moreover, transition of patterns was monitored using the map. Figure 9 shows nine paths connecting a node k matched to data of time t to the other node $k+1$ matched to data of time $t+0.2$, which indicate process image changing with time. Through monitoring the paths in the map, it was thought that change of the process pattern could be analyzed from macroscopic viewpoint of cluster. The analysis of the process pattern's transition will be described in the later subsection 4.3.

The next, cluster maps changing with impeller's position were analyzed. In the analysis, two sets of 30 images for the cases that values of d were 45 and 60 were prepared. It was estimated by simulations that preferable number of clusters was five for the case that d was 45 mm, as shown in Figure 10. In the case when d was 60 mm, it was estimated that preferable cluster count was four. The both indicators for the two cases were close to 12.

In three maps of Figure 10, the cluster marked by

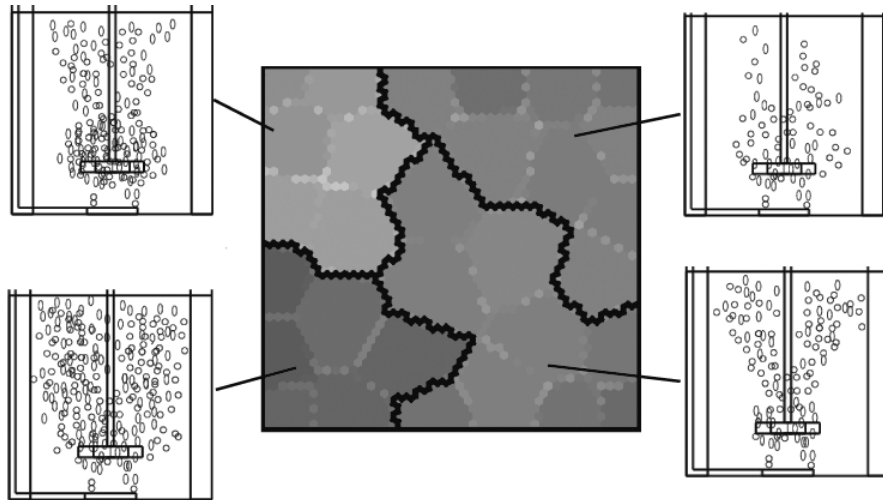


Figure 8. Schematic diagram of four clusters and representative patterns of bubble dispersion

“A” represents a group of images where bubbles are well dispersed. When areas of cluster A for three maps were compared, it was seen that the area for the case that d was 45 mm was the largest. So it was interpreted that the height that d was 45 mm was appropriate position of the impeller for this aerated agitation process. Because this interpretation by the SOM was not irrelevant as compared to a prior knowledge for the aerated agitation vessel, it was considered that the SOM could give process engineers visible and intelligible information for design of the aerated agitation vessel.

4.2. Data processing based on phenomenological approach

In this subsection, robustness of the described application method for the SOM is discussed in focusing on change of the rotational speed of impeller that is one of operational variables. For the position of impeller, d was fixed at 45 mm. A new map was generated using 30 images acquired in the case when N was 250 rpm. The computation resulted in three clusters of which indicator was not low, 22. On the other hand, most of the nodes were classified into one cluster, which was regarded as a group of “well-dispersion” patterns. When the images processed by PIV were observed, it was considered that noise that increased with increase of mixing rate affected generation of a flat map. It was because that the noise problem was disadvantage for application of image recognition based on velocity vector.

Thus we tried to use a high-speed video camera in the direct imaging. The high-speed video camera was DigiMo VCC-500C that had performance of high

frame rate, 500 fps. In this article, the frame rate was set at 90 fps that was three times rate of the previous camera. Moreover, the analytical region was reduced from 9x23 cells to 7x15 cells, because resolution decreased with increase of the frame rate. A map, which was generated from 30 images recorded by the VCC-500C, could be separated into three clusters as depicted by Figure 11. Indicator of this clustering count was 31 and larger than the result of 30 fps. It, however, seemed that difference of patterns between two clusters of three ones was not clear from point of the phenomenological view.

In order to generate a map where difference between clusters was comprehensible, modification of “priority factor” was adopted in the data processing. In the Viscovery[®] SOMine, the priority factor gives

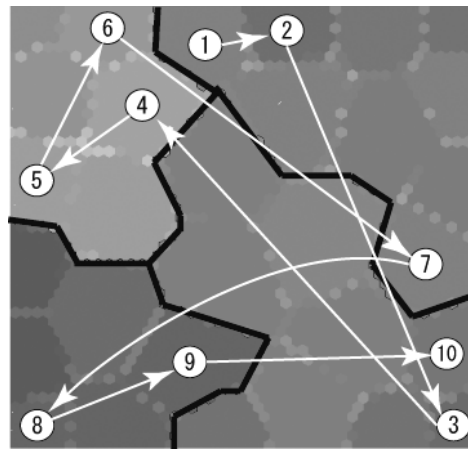


Figure 9. A result of transition of process patterns

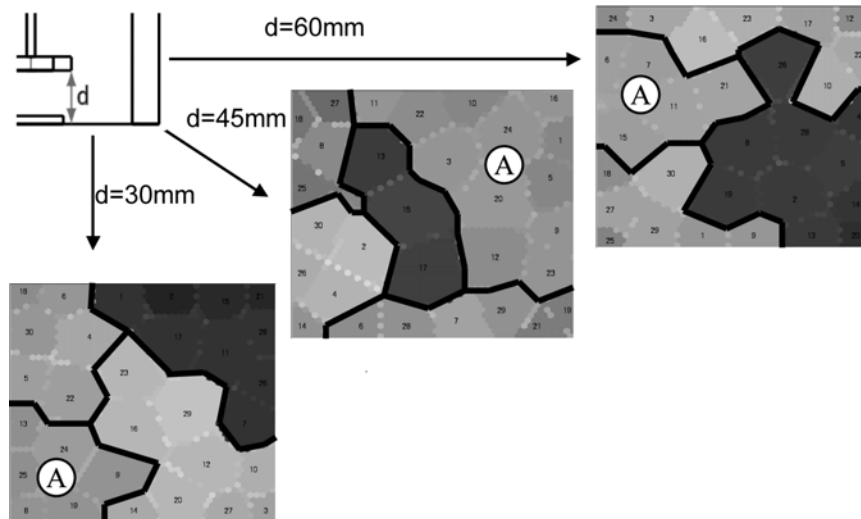


Figure 10. Comparison of three maps of different position of impeller

additional weight to a component by multiplying its internal scale by that factor. If the priority factor is set at a number less than 1, this component will be squeezed, and thus becomes less relevant for the training process. As examining velocity distribution estimated by PIV, it was seen that time-averaged magnitudes of velocities were small in the regions near the impeller and the wall of vessel as depicted in the left part of Figure 12. It was thought that the reasons might be due to three-dimensional complex flow pattern near the impeller and low quantity of airflow near the wall.

Thus, as based on the phenomenological insight into the flow pattern, the priority factor of a part of

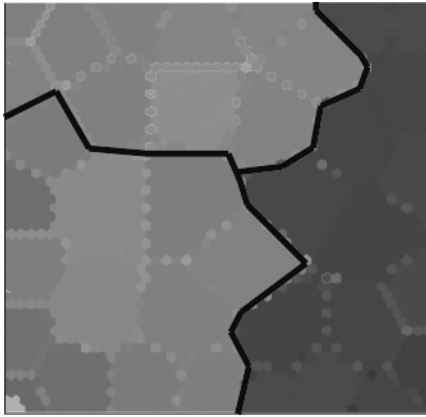


Figure 11. A Map that was generated from frames recorded by the high-speed video camera

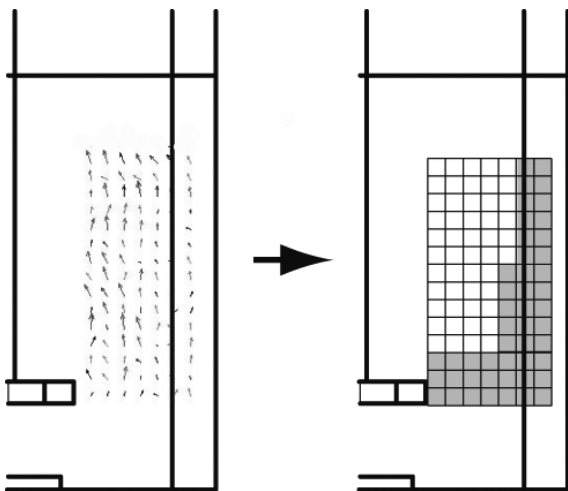


Figure 12. Schematic diagrams of velocity distribution and modification of the priority factors

components, which were represented by grey cells in the right part of Figure 12, was modified from 1 to 0.5. The partial reduction of the priority factor brought about a map that could be separated into three clusters, as shown in Figure 13. Two schematic diagrams of flow patterns around the map show that one cluster represents a group of “poor-dispersed” patterns and the other two clusters represent groups of “well-dispersed” patterns. Moreover, we could distinguish the two clusters for “well-dispersed” patterns into a group of intensive flows of bubbles and another group of their tender flows. Since indicator of the clustering map was 18 and became lower than the map without the modification, it was considered that the clustering was “artificial” for the map, however the clusters were “comprehensible”.

4.3. Data processing based on statistical approach

In the previous subsection 4.1, 30 images were prepared for the mapping in the case when N was 200 rpm. The number of images was determined based on the length of a period of torque fluctuation, but it was uncertain that the number was appropriate for mapping in this process. Thus effect of the number of prepared data on efficiency of mapping was investigated for the case that d was 45 mm. 90 images were extracted from the same moving images used previously, and then were computed by the SOMine. The computation

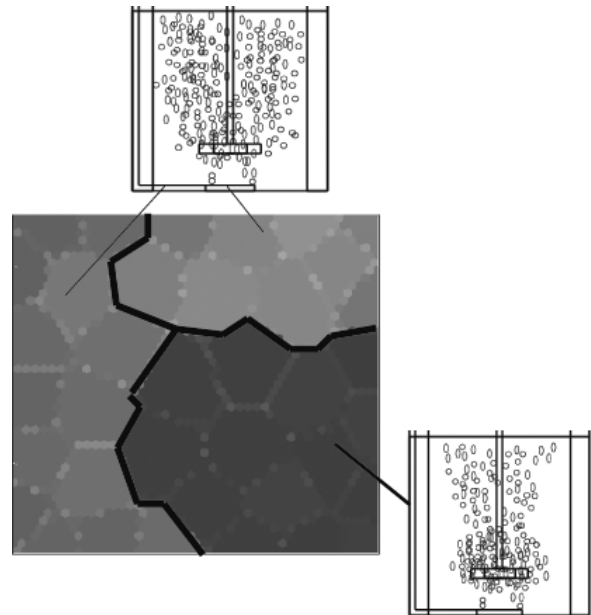


Figure 13. A result of modification of the priority factors

generated a map separated into three clusters as shown in Figure 14. As compared with the result of 30 images (Figure 10), preferable cluster count was reduced from five to three, and the indicator 30 of the clustering was higher than the previous indicator. It was considered that the 30 images were not sufficient for natural clustering of the process patterns.

Then magnitudes of velocities for all the 207 cells were averaged in each cluster, in order to investigate quantitatively distinction of the three clusters. It was thought that large and small magnitudes of the velocities could be correlated to many and few bubbles. Figure 15 shows remarkable difference of the averaged velocity V_{av} between the cluster C and the other one in the cells of no. 100-125. The cluster C could be characterized as a group of “poor-dispersed” patterns by observation of the frames, and therefore it was estimated that the poor dispersion was discerned by being few bubbles in the middle part of the computational domain shown in Figure 4. In Figure 15, the clusters A and B could be distinguished by the difference of number of bubbles in the upper part of the computational domain, whereas the distinction was difficult in the lower part. It was supposed that the difficulty of distinction resulted from complicated flow near the impeller.

Hence we applied a transformation to influence the density characteristics of a component’s distribution. In this article, the Sigmoid-typed transformation was adopted to redefining the internal representation of a component. The sigmoid function can lead to a more balanced distribution by stretching the center of the data histogram. The gradient and offset of the sigmoid transformation can be used to reduce the impact of

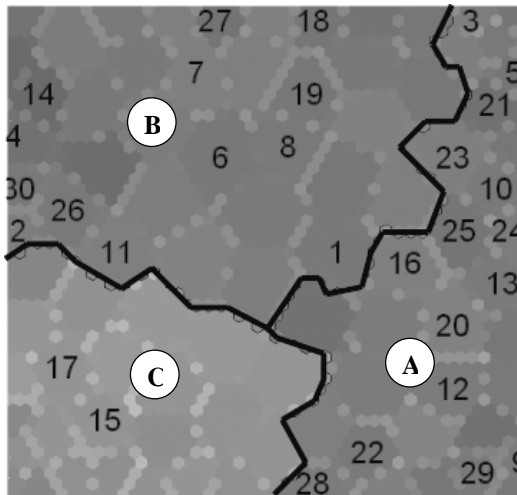


Figure 14. A map generated from 90 process images

outliers on the training process.

In the case when the gradient was set at 1 and the offset was zero, the generated map could be also separated into three clusters as depicted by Figure 16. As compared with Figure 14, area of the cluster C representing a group of “poor-dispersed” patterns was reduced in the map generated by the modified data. Distinction of the cluster C shown in Figure 17 was considered to be close to the case of “no transformation” (Figure 15) in few bubbles in the middle part of the analytical domain. Furthermore, the clusters A and B could be distinguished by the difference of number of bubbles in both of the upper and lower parts of the computational domain. It was considered that the nonlinear transformation could enhance an efficiency of separating the minor difference in the nodes representing the “well-dispersion” patterns.

Finally, we investigated distribution of initial 30 data in the three clusters by counting the numbered nodes in each cluster. It seemed that the numbered nodes in the map of Figure 16 were distributed uniformly in the three clusters, as compared with Figure 14. Thus, transition of patterns was tracked to analyze an effect of the data modification on dynamic behavior of patterns that the SOM showed. More periodic transition of pattern of bubble flow among the three clusters was monitored in the case of application of the sigmoid transformation as shown in Figure 18. So it was expected that data processing based on the statistical approach would generate a clustered map that was comprehensible for monitoring and control of the aerated agitation process.

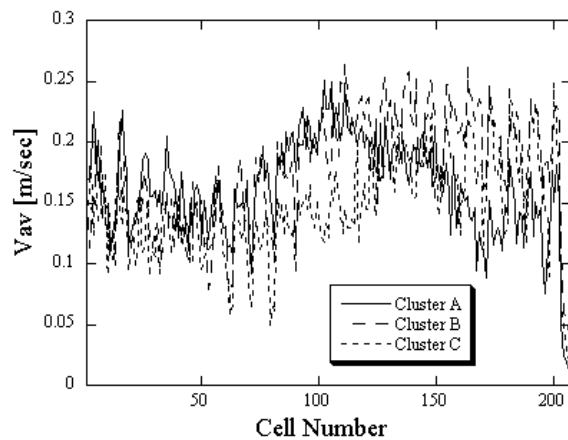


Figure 15. Distributions of averaged velocities for three clusters

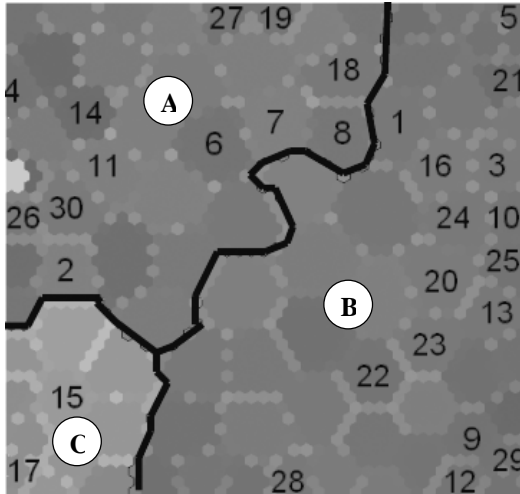


Figure 16. A map generated from data modified by sigmoid transformation

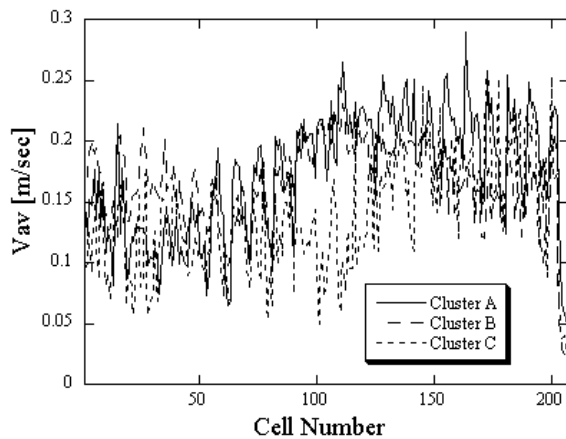


Figure 17. Distribution of averaged velocities for three clusters in data modification

5. Conclusions

In application of the batch SOM to process imaging for dynamic behavior of aerated agitation vessel, the direct imaging by CCD video camera and the PIV technology were adopted. As a result of mapping time-series patterns of velocity distributions to two dimensions, it was considered that generated map and clusters could give process engineers useful information about degree of spatial dispersion of bubbles and about determination of design parameter, e.g. position of the impeller.

Then two approaches for the data processing in the SOM were investigated to enhance efficiency of pattern analysis. One was phenomenological approach.

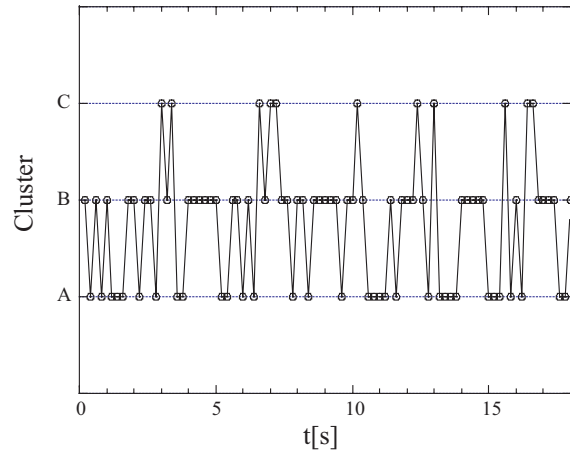


Figure 18. A result of analysis of pattern transition in the case when sigmoid transformation was adopted

When the priority factors in a part of analytical domain were reduced from the point of phenomenological view, the map with more comprehensible clusters was generated. Another one was statistical approach. By adopting sigmoid transformation in the data processing, it was seen that the data modification enhanced the efficiency of separating the minor difference in the nodes representing the “well-dispersion” patterns.

Moreover, through the simulations, it was demonstrated that the data-oriented preprocessing could give process engineers useful information about transition of process patterns from the viewpoint of cluster. In the future, it is necessary to investigate distinction between the SOM based method and the statistical method, e.g. PCA. In the comparison with the other methods, it is important to examine application of the generated maps to estimation of dynamic process behavior and to control the process.

References

- [1] G. Martin, “Consider Soft Sensors”, *Chemical Engineering Progress*, AIChE, New York, 1997, pp. 66-70.
- [2] N.K. Read, S.X. Zhang, and W.H. Ray, “Simulation of a LDPE Reactor using Computational Fluid Dynamics”, *AIChE J.*, John Wiley & Sons, New Jersey, 1997, pp. 104-117.
- [3] H. Matsumoto and C. Kuroda, “Numerical Simulation of Dynamic Behavior in a Reactor using a Hybrid Model”, *Theoretical and Applied Mechanics Japan*, Hokusen-sha, Tokyo, 2002, pp. 301-305.
- [4] Scott, D.M. and H. McCann, *Process Imaging for Automatic Control*, CRC Press, Florida, 2005.

- [5] M. Wang, A. Dorward, D. Vlaev, and R. Mann, "Measurements of Gas-Liquid Mixing in a Stirred Vessel using Electrical Resistance Tomography", *Chem. Eng. J.*, Elsevier, Amsterdam, 2000, pp. 93-98.
- [6] D. Schmitz and D. Mewes, "Tomographic Imaging of Transient Multiphase Flow in Bubble Column", *Chem. Eng. J.*, Elsevier, Amsterdam, 2000, pp. 99-104.
- [7] T. Dynakowski, T. York, M. Mikos, D. Vlaev, R. Mann, G. Follows, A. Boxman, and M. Wilson, "Imaging Nylon Polymerization Process by Applying Electrical Tomography", *Chem. Eng. J.*, Elsevier, Amsterdam, 2000, pp. 105-109.
- [8] C. Citir, Z. Aktas, and R. Berber, "Off-Line Image Analysis for Froth Flotation of Coal", *Computers Chem. Engng.*, Elsevier, 2004, Amsterdam, pp. 625-632.
- [9] J.J. Liu, J.F. MacGregor, C. Duchesne, and G. Bartolacci, "Flotation Froth Monitoring using Multiresolutional Multivariate Image Analysis", *Minerals Engineering*, Elsevier, Amsterdam, 2005, pp. 65-76.
- [10] Kohonen, T., *Self-Organizing Maps (the Japanese language edition)*, Springer, Tokyo, 2001.
- [11] S.-L. Jämsä-Jounela, M.V. Vermasvuori, P. Endén, and S. Haavisto, "A Process Monitoring System Based on the Kohonen Self-Organizing Maps", *Control Engineering Practice*, Elsevier, Amsterdam, 2003, pp. 83-92.
- [12] J. Abonyi, S. Nemeth, C. Vincze, and P. Arva, "Process Analysis and Product Quality Estimation by Self-Organizing Maps with an Application to Polyethylene Production", *Computers in Industry*, Elsevier, Amsterdam, 2003, pp. 221-234.
- [13] H.L. García and I.M. González, "Self-Organizing Map and Clustering for Wastewater Treatment Monitoring", *Engineering Applications of Artificial Intelligence*, Elsevier, Amsterdam, 2004, pp. 215-225.
- [14] J.S.J.V. Deventer, D.W. Moolman, and C. Aldrich, "Visualization of Plant Disturbances using Self-Organizing Maps", *Computers Chem. Engng.*, Elsevier, Amsterdam, 1996, pp. 1095-1100.
- [15] J.I. Rhee, K-I. Lee, C-K. Kim, Y-S. Yim, S-W. Chung, J. Wei, and K-H. Bellgardt, "Classification of Two-Dimensional Fluorescence Spectra using Self-Organizing Maps", *Biochem. Eng. J.*, Elsevier, Amsterdam, 2005, pp. 135-144.
- [16] K-I. Lee, Y-S. Yim, S-W. Chung, J. Wei, and J.I. Rhee, "Application of Artificial Neural Networks to the Analysis of Two-Dimensional Fluorescence Spectra in Recombinant E Coli Fermentation Processes", *J. Chem. Technol. Biotechnol.*, John Wiley & Sons, New Jersey, 2005, pp. 1036-1045.
- [17] *Viscovery SOMine Version 4.0 – User's Manual*, Eudaptics software GmbH, Vienna, 2001.